



Graphene oxide/chitosan doped polysulfone membrane for the treatment of industrial wastewater

Ahmed T. Yasir^{1,2} · Abdelbaki Benamor^{1,2} · Alaa H. Hawari³ · Ebrahim Mahmoudi⁴

Received: 15 January 2023 / Accepted: 9 May 2023 / Published online: 24 May 2023
© The Author(s) 2023

Abstract

Rapid urbanization and industrialization have created tremendous stress on fresh water sources. Moreover, discharge of industrial wastewater has left public health and environment under high potential risks. In this paper, chitosan-functionalized graphene oxide (GO-CH) was synthesized and incorporated into polysulfone (Psf) ultrafiltration membranes. The concentration of the nanocomposite and the ratio of GO to CH in the nanocomposite were varied to produce different GO-CH doped polysulfone membranes. The effect of GO-CH addition on the morphology and membrane performance was studied through water contact angle, scanning electron microscopy, atomic force microscopy, porosity, pore size, and permeation measurements as well as rejection and antifouling tests, while produced GO-CH nanocomposite was characterized using FTIR and XRD analyses. The GO-CH/Psf membrane exhibited higher water flux, bovine serum albumin (BSA) rejection rate, and water flux recovery ratio, and lower BSA solution flux attenuation rate than pristine Psf membrane. GO-CH/Psf membrane containing 0.085 wt% nanocomposite with GO to CH ratio of 1 to 0.01 had an improved permeate flux of 136%. Maintaining the same GO-CH composition of 0.085 wt% and changing GO to CH ratio to 1:1 resulted in better hydrophilicity (contact angle 68°) and increased reversible fouling from 23 to 33%. The best membrane was further tested with real industrial wastewater obtained from a GTL plant in Qatar showed 28% improvement in COD removal.

Keywords Polysulfone membrane · Graphene oxide · Chitosan · Ultrafiltration · Water treatment

1 Introduction

One of the major drawbacks of membrane filtration process is the irreversible membrane fouling caused by high membrane hydrophobicity. Simple cleaning protocols are often not sufficient to remove the foulants, and toxic chemicals are required to clean and maintain the membrane performance [1]. To improve the anti-fouling properties of membranes, metal oxides, organic, and inorganic nano-fillers blended

with sustainable polymers have been suggested [2]. Graphene oxide (GO) is a promising nano-filler that has been effectively used to improve membrane hydrophilicity and surface roughness which has resulted in reduction of irreversible fouling [3].

Graphene oxide (GO) is a two-dimensional material derived from the parent graphene skeleton by introducing several oxygen features. Graphene oxide (GO) has become a widely used material by researchers due to its excellent mechanical [4], electrical [5], thermal [6], and optical properties [7]. Apart from hydrophilicity has a high surface area, graphene oxide is an amphiphilic material with an overall negative charge under normal conditions. The charge can be reversed by covering GO with polycationic reagents such as polymers or dendrimers. GO is not harmful for the environment, and its toxicity in cells is generally moderate to low concentrations (10 µg/ml). Graphene oxide contains multiple hydrophilic functional groups, including hydroxyl, carboxylic acid, and epoxies which makes GO a favorable nano-filler in the preparation and modification of polymeric membranes [8].

✉ Abdelbaki Benamor
benamor.abdelbaki@qu.edu.qa

¹ Gas Processing Center, College of Engineering, Qatar University, 2713 Doha, Qatar

² Department of Chemical Engineering, College of Engineering, Qatar University, 2713 Doha, Qatar

³ Department of Civil and Architectural Engineering, Qatar University, 2713 Doha, Qatar

⁴ Department of Chemical and Process Engineering, Universiti Kebangsaan Malaysia, Selangor, Malaysia

Chitin is the most abundant of the renewable polysaccharides in the marine environment and one of the most abundant on Earth after cellulose. Chitosan a main derivative of chitin is a natural polymer that has been extensively studied due to its specific properties including high chemical resistance, good physical properties, and high adsorption potential and low cost. Chitosan (CH) is an eco-friendly material that is biodegradable with important hypotoxicity and anti-microbial properties [9]. The presence of OH and NH₂ groups on the surface of CH makes it hydrophilic in nature. Chitosan can bind to heavy metal due to the presence of hydroxyl and amine groups in its structure. However, its sensitivity to pH, low thermal stability and low mechanical strength are remarkable drawbacks that limit its application in wastewater treatment.

Ionita et al. reported the improvement of thermal and mechanical stability of polysulfone membrane by incorporating GO in the membrane matrix [10]. Xu et al. reported improved hydrophilicity, permeate flux, and protein rejection after modification of PVDF membrane with GO [8]. Lee et al. reported 5 folds increase in polysulfone membrane life time after incorporating GO in the membrane matrix [11]. Zhi et al. suggested functionalization of GO to reduce the particle–particle interaction and prevent agglomeration of GO nano-particles [12]. Vatanpour et al. functionalized GO with boron nitride and silver and created FBN-GO-Ag nanocomposite and blended the nanocomposite in a polyether sulfone (PES) UF membrane [13]. Modification of the PES membrane with 1 wt% FBN-GO-Ag nanocomposite improved the hydrophilicity, porosity, permeability, and reactive black 5 rejection by 21%, 22%, 40%, and 8.3%, respectively. Zhang et al. functionalized reduced GO (rGO) with ZnO and synthesized rGO-ZnO nanocomposite and blended the nanocomposite in a PES membrane [14]. The surface of the fabricated membrane was then grafted with zwitterionic hydrogel. These modifications reduced biofouling by 70%. Baig et al. synthesized a TiO₂-GO nanocomposite and blended the nanocomposite in the active polyamide (PA) layer of a thin film nanocomposite (TFN) membrane [15]. The incorporation of 1 wt% TiO₂-GO nanocomposite improved the membrane hydrophilicity and surface roughness by 50% and 565%, respectively. Ng et al. reviewed the recent developments of the GO nanocomposites and their application in polymeric membranes [16].

The combination of graphene and chitosan allows us to obtain new materials with new properties and with improved adsorption performance. Silvestro et al. modified chitosan membrane with GO for solid state extraction of pesticides [17]. They found out that increasing GO concentration resulted in improved mechanical properties of the membrane against a deterioration of thermal stability of the membrane. However, at high GO concentrations, agglomeration of nanoparticles on the membrane surface led to a reduction of the

hydrophilic functional groups on the membrane surface [18]. To the best of our knowledge, the application of combined GO-CH nanocomposite to modify nanofiltration (NF) membranes was reported only for polyether sulfone (PES) membrane used to remove CrSO₄ from synthetic wastewater [18].

In this work, chitosan (CH) was used to functionalize GO nanoparticles in order to reduce their agglomeration and improve their dispersion in the membrane matrix. GO-CH multifunctional nanocomposite was synthesized and used to modify polysulfone (Psf) ultrafiltration (UF) membranes, which were tested for their water permeation, porosity, and fouling. The modified membranes were tested for the rejection of COD from real produced water obtained from oil and gas industry in Qatar. It was found that adding 1 wt% GO-CH nanocomposite to the membrane matrix resulted in 48% reduction in the surface roughness and 43% improvement in the membrane hydrophilicity. Synthesized nanocomposites and modified membranes were characterized using FTIR, XRD, SEM, and AFM techniques.

2 Methodology

2.1 Materials

2.1.1 Chemicals

Extra pure, fine graphite powder (99%), sodium nitrate (NaNO₃, 99.9%), potassium permanganate (KMNO₄, 99%), sulfuric acid (H₂SO₄, 98%), polysulfone pellets (99%, Mw 35,000), dimethylformamide (DMF) (99.9%), chitosan (95% deacetylation), and bovine serum albumin (BSA, 99%) were all purchased from Sigma Aldrich. The industrial wastewater used for rejection study was obtained from the Pearl GTL plant located in Qatar.

2.1.2 Industrial wastewater

The COD, TOC, pH, and conductivity of the industrial wastewater collected from a GTL plant in Qatar were analyzed. The COD and TOC were measured using AQUAfast COD Colorimeter (Orion AQ2040, Thermo Scientific, US) and TOC-L (Shimadzu, Japan), respectively. Before measuring COD and TOC, the water samples were diluted four times. The pH and conductivity were measured using APHA 4500-H⁺ B. Electro-metric method and APHA 2510 B. Conductivity. The characteristic of the industrial wastewater is summarized in Table 1.

2.2 Synthesis of GO

The graphene oxide (GO) was synthesized following the modified Hummer's methods that has been previously used

Table 1 Characteristics of the industrial wastewater

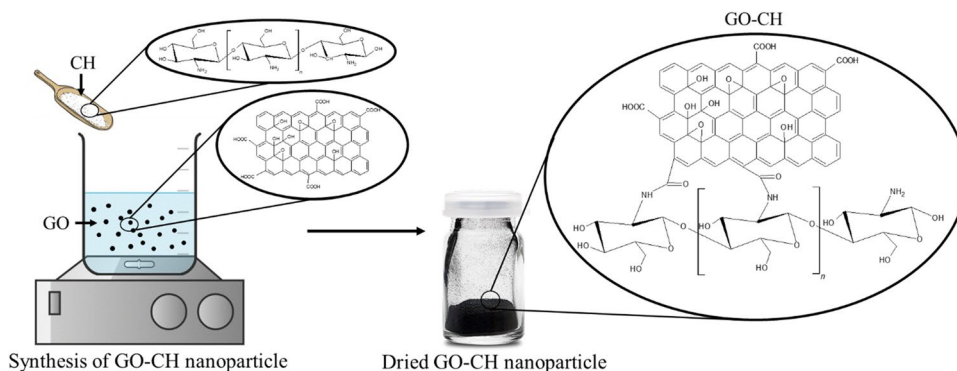
Characteristic	GTL process water
COD (mg/L)	5000–7000
TOC (mg/L)	1500–1700
pH	2.9
Conductivity (mS/m)	0.435

by Mahmoudi et al. (2015) [1]. Initially, 115 mL sulfuric acid was taken in a round bottomed flask where 2.5 g NaNO_3 and 5 gm graphite powder was added. The mixture was then stirred for 30 min in an ice bath until the temperature of the mixture reached 10 °C. While maintaining this temperature for 2 h, 15 g KMNO_4 was added slowly. Then, the temperature was increased to 35 °C and maintained for 1 h. Then, 230 mL distilled water was added to the round bottomed flask slowly while maintaining the internal temperature of the mixture below 100 °C. The solution was then stirred for 1 h followed by addition of 300 mL distilled water. The process was completed by adding 10 mL 30% H_2O_2 that changed the color of the mixture to brilliant yellow and reduced the residual KMNO_4 . The mixture was then cleaned by centrifugation and washed with HCl before GO powders were obtained by freeze drying.

2.3 Preparation of GO-CH multifunctional composite

The freeze dried GO powder was functionalized with chitosan flowing the method described by Shao et al. (2013) [2]. First, an appropriate amount of GO was dispersed in a 2% acetic acid aqueous solution. Then, appropriate amount of CH was added to the mixture and stirred for 5 h to complete the functionalization process. The mixture was centrifuged and washed with ethanol before vacuum drying at 60 °C. In this study, three different ratios of (1:0.1, 1:0.5, and 1:1) multifunctional GO-CH composite have been synthesized. Figure 1 summarizes the GO functionalization process.

Fig. 1 Schematics of the GO functionalization process and the synthesized GO-CH composite



2.4 Membrane fabrication

The GO-CH doped polysulfone membranes were prepared by phase inversion method. To prepare the casting solution, appropriate amount of polysulfone was added to 30 mL of the DMF solution and stirred continuously at 300 rpm and at 80 °C for 2 h. This low stirring speed was deemed suitable for preventing formation of gas bubbles in the casting solution. In another beaker, an appropriate amount of GO-CH multifunctional composite was dispersed in 5 mL of DMF solution and ultrasonicated for 30 min. The two solutions were then mixed together and stirred at room temperature for 12 h. To produce the membrane film, a small amount of the prepared casting solution was poured and evenly dispersed on a glass pate using filmographe doctor blade (Braive Instrument, Germany). The membrane thickness was controlled via the distance between the blade and the glass plate which was fixed at 0.3 mm. Once the casting solution was dispersed evenly on the glass plate, the glass plate was transferred to a distilled water bath where the phase inversion process was completed. The obtained membrane was peeled off from the glass plate and rinsed with distilled water for 30 min. Seven different membranes were casted following the same procedures. The components and composition of the different synthesized membranes are summarized in Table 2.

2.5 Characterization of prepared GO-CH multifunctional composite

The functional groups present on the multifunctional nanocomposite were analyzed using a Nicolet 6700 FTIR spectrometer (Thermo Fisher Scientific Inc., MA). Moreover, the crystal phase composition of the nanocomposite was also analyzed using XRD (Bruker D8 Advance, Germany) with $\text{CuK}\alpha$ radiation (1.5406 Å) in the 2 h scan range of 20–80°. The zeta potential of the synthesized nanoparticles was determined using Zetasizer Nano ZS90 Analyzer.

Table 2 Composition of the membrane casting solution

Membranes	DMF (wt%)	Psf (wt%)	GO:CH (ratio)	GO-CH (wt%)*
GC-0	83	17	0:0	0
GC-1	83	17	1:0.5	0.034
GC-2	83	17	1:0.5	0.085
GC-3	83	17	1:0.5	0.136
GC-4	83	17	1:0	0.085
GC-5	83	17	1:1	0.085
GC-6	83	17	1:0.1	0.085

*Calculated based on Psf (wt%)

2.6 Characterization of the fabricated membrane and performance analysis

2.6.1 Surface morphology analysis

The surface and cross-sectional morphology of the membrane was characterized by atomic force microscopy (AFM) and field emission scanning electron microscope (FESEM), respectively. To carry out AFM analysis, a multimode AFM with Nanoscope IIIa controller (Veeco, USA) was used under ambient conditions using tapping mode with TESP cantilevers (Bruker AXS). The scanned area in AFM was $10 \times 10 \mu\text{m}^2$.

The cross-section of the pristine and modified membranes was examined using FESEM (Gemini model SUPRA 55VP-ZEISS, Oberkochen, Germany). To expose the cross-sections, the membranes were solidified and fractured under liquid nitrogen. The cross-sectional SEM images were also used to measure the thickness of the synthesized membranes.

2.6.2 Membrane permeate flux, porosity, pore size, and resistance analysis

The permeation tests were performed using a stirred dead-end cell operated at transmembrane pressure of 4 bars. Before all filtration studies, the membranes were compacted for 30 min at 4 bars. While operating the dead-end cell, the pure water permeate flux (J , LMH) was calculated as:

$$J = \frac{w_t - w_o}{A \times d_w \times \Delta t} \quad (1)$$

Here, w_o , w_t , Δt , A , and d_w correspond to initial mass of the permeate water (gm), mass of the permeate water at time t (gm), filtration time (sec), surface area of the membrane (cm^2), and density of water (1 gm/cm^3), respectively. The porosity (ϵ) of the membrane was determined using the gravimetric method and calculated as:

$$\epsilon = \frac{\omega_1 - \omega_2}{A \times l \times d_w} \quad (2)$$

Here, ω_1 , ω_2 , A , l , and d_w correspond to weight of the wet membrane (gm), weight of the dry membrane (gm), and thickness of the membrane (cm), respectively. The pore radius (r_m) of the membranes was calculated using the porosity and Guerout–Elford–Ferry equation:

$$r_m = \frac{(2.9 - 1.75\epsilon)8\eta l Q}{\epsilon \times A \times \Delta P} \quad (3)$$

Here, η , Q , and ΔP correspond to viscosity of water ($8.9 \times 10^{-4} \text{ Pa.s}$), volume of the permeated pure water per unit time (m^3/s), and the operating pressure (Pa), respectively. The membrane resistance (R_m , m^{-1}) was calculated as:

$$R_m = \frac{\Delta P}{\mu J} \quad (4)$$

Here, μ corresponds to the dynamic viscosity of water (0.000891 Pa.s @ 25°C).

2.6.3 Membrane fouling analysis

The fouling study was conducted using a solution of 2000 ppm BSA as model foulant. For each membrane, three dynamic cycles were conducted in the dead-end setup. Initially, the pure water steady state flux (J_{w0}) was measured at 4 bars; then, the feed was changed to the BSA solution where filtration was carried out for 1 h 30 min and the permeate flux was (J_{wf}) measured at the end. After the BSA filtration stage, the membrane was washed twice with distilled water and the pure water steady state permeate flux (J_{w1}) was measured again at 4 bars. Using the data obtained at this stage, the total fouling ratio (R_t), flux recovery ration (FRR), the reversible fouling ratio (R_r), and the irreversible fouling ratio (R_{ir}) were calculated as:

$$R_t = \frac{J_{w0} - J_{wf}}{J_{w0}} \times 100\% \quad (5)$$

$$FRR = \frac{J_{w1}}{J_{w0}} \times 100\% \quad (6)$$

$$R_r = \frac{J_{w1} - J_{wf}}{J_{w0}} \times 100\% \quad (7)$$

$$R_{ir} = \frac{J_{w0} - J_{w1}}{J_{w0}} \times 100\% \quad (8)$$

The second and third cycles were repeated following the above discussed methodology. The BSA rejection performance of the synthesized membranes was evaluated by

using a UV–VIS spectrophotometer (UV-2700, Shimadzu) at 278 nm.

2.6.4 Industrial wastewater treatment

The industrial wastewater from shell was treated using the dead-end cell setup. The UF process was carried out at 4 bars. The COD concentration of the industrial wastewater before filtration, (COD_i), and after filtration (COD_f) was measured using AQUAfast COD Colorimeter (Orion AQ2040, Thermo Scientific, US). The COD rejection (R_{COD}) was calculated as:

$$R_{COD} = \frac{COD_i - COD_f}{COD_i} \times 100\% \quad (9)$$

For each membrane, all testes were repeated three times and their average was considered in this work while the standard deviation is indicated by the error bars.

3 Results and discussion

3.1 Characterization of the GO-CH multifunctional composite

The characterization of the GO-CH nanocomposite was done using FTIR and XRD analysis. The FTIR analysis for GO, CH and GO-CH (1:0.05) nanocomposite is shown in Fig. 2. In the GO curve of Fig. 2, the absorption bands at 602, 756, and 1070 cm^{-1} correspond to skeletal vibration of C=C [3]. Whereas, the absorption bands at 1107, 1384, 1630, 1725, and 3381 cm^{-1} correspond to the presence of epoxy groups, carboxyl bending vibration, C=C stretching, and stretching vibration of oxygen containing functional group

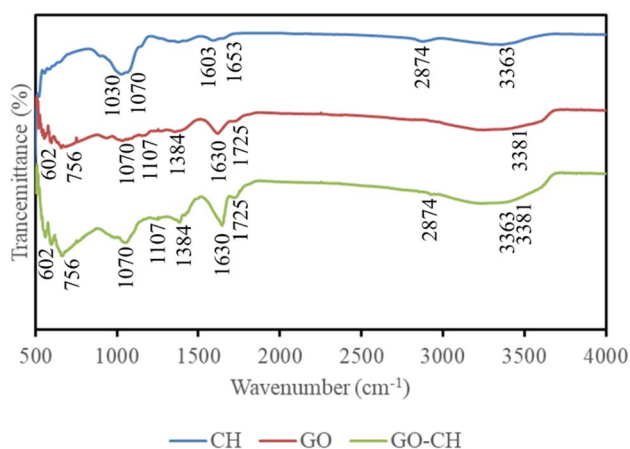


Fig. 2 FTIR spectra of GO, CH, and GO-CH nanocomposite. The marked circles show the most prominent peaks

and hydroxyl group, respectively [4]. For CH curve, the absorbance bands observed at 1030 and 1070 correspond to C–O–C vibration, 1603 and 1653 correspond to N–H bending vibration, 2874 corresponds to C–H stretching vibration, and 3363 corresponds to O–H and N–H stretching vibration [5, 6]. Finally, in Fig. 2, the absorbance band of GO-CH nanocomposite shows presence of all the above-mentioned bands found in individual CH and GO curves; thus, confirming functionalization of GO by CH.

The X-ray diffraction (XRD) of the synthesized GO and CH functionalized GO is shown in Fig. 3. The synthesized GO showed a characteristic peak at about 10.89°, which corresponds to a 8.32 Å distance between the GO layers which is formed due to the presence of OH functional group on the surface of the GO nanoparticle [7]. With increasing the concentration of CH in the nanocomposite, the characteristic peak of GO reduced significantly. This confirms the interaction between GO and CH particles.

The surface functionalization of GO with CH was further demonstrated by zeta potential analysis as shown in Fig. 4. Within the tested range of 3 to 11.5 pH, the GO particles showed negative zeta potential, and the zeta potential of the

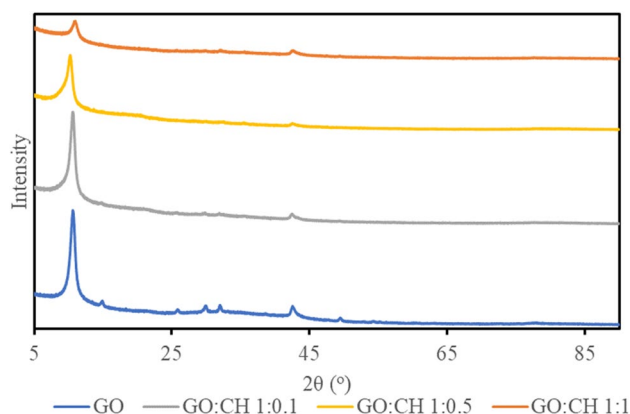


Fig. 3 XRD spectrum of the synthesized nanocomposite

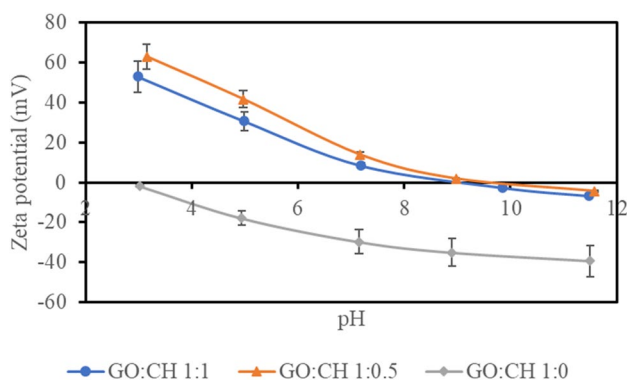


Fig. 4 Zeta potential of the synthesized nanocomposites

functionalized GO-CH nanocomposites was higher than that of the GO nanoparticle. This is because the GO nanoparticle contains large number of oxygen containing sites on its surface, whereas addition of CH imparts nitrogen containing groups on the GO surface, resulting in increased zeta potential.

The results from FTIR, XRD, and zeta analysis prove the functionalization of GO with CH. When used along with GO, protonated amino groups of CH interacted with the negatively charge GO sheet and formed chemical or physical cross-linking. This resulted in a formation of a strong hybrid structure though hydrogen bonding or π stacking [8, 9]. The apparent structure of the GO-CH nanocomposite is shown in Fig. 1.

3.2 Characterization of the modified membrane

As shown in Table 3, the contact angle of the pristine membrane (GC-0) is 87.4° . Increasing the GO-CH concentration from 0.034 wt% (GC-1) to 0.136 wt% (GC-3) at a constant GO:CH ratio of 1:0.5 decreases the contact angle from 84.2° to 75.2° . Whereas, increasing the GO:CH ratio from 1:0.5 (GC-2) to 1:1 (GC-5), while keeping the GO-CH concentration constant at 0.085 wt% reduces the contact angle from 81.0° to 68.7° . The results indicate that increasing the GO-CH concentration and the GO:CH ratio decreases the contact angle indicating improvement of hydrophilicity of the synthesized membranes; this is due to the fact that GO is rich in hydroxyl and carboxylic acid groups and CH is rich in hydroxyl and amine groups.

The porosity and pore radius of the modified membranes were measured using the gravimetric method described in Sect. 2.3. To study the effect of GO-CH concentration on the porosity and pore radius, the GO:CH ratio was fixed at 1:0.05; the GO-CH concentration was varied between 0, 0.034 wt%, 0.085 wt%, and 0.136 wt%; and the results are given in Table 3. As seen from Table 3, increasing the concentration of the GO-CH nanocomposite from 0 (GC-0) to 0.085 wt% (GC-2), the porosity of the membrane was improved from 57.35% to 62.25%. However, when the GO-CH concentration was increased to 0.136 wt% (GC-3), the porosity decreased to 53.52%.

Initially, the presence of nanocomposites improves mass transfer rate and promotes formation of voids in the membrane matrix; hence, improving membrane porosity. However, at higher GO-CH concentration, the viscosity of the casting solution increases, which results in decreased mass transfer rate during the phase inversion process leading to lesser pore formation. Similar trend was observed during pore radius measurements, which was 11.41 nm for the pristine membrane (GC-0) and increased to 12.28 nm after imbedding 0.085 wt% (GC-2) GO-CH in the membrane. Increasing the GO-CH concentration to 0.136 wt% reduced the pore radius to 9.84 nm. The initial increase of pore radius is attributed to the improved mass transfer rate during the phase inversion process. Whereas the reduction in pore size is attributed to the increased viscosity of the casting solution.

The effect of GO:CH ratio in the nanocomposite on the porosity and pore radius was also studied by keeping the GO-CH concentration constant at 0.085 wt%, while altering the GO:CH ratio between 1:0, 1:0.01, 1:0.05, and 1:1. The results of this study can be seen in Table 3. As seen in Table 3, decreasing the GO:CH ratio from 1:0.05 (GC-2) to 1:0 (GC-4) did not change the pore size and porosity significantly and only decreases the pore size and porosity by 1.3% and 0.25%, respectively. Increasing the GO:CH ratio to 1:0.1 (GC-6) did not affect the porosity significantly but increased the pore radius to 14.15 nm. However, further increment of GO:CH ratio to 1:1 decreased the porosity and the pore size to 60.57% and 10.38 nm, respectively. Initially, increasing the GO:CH ratio from 1:0 to 1:0.1 reduced agglomeration of the GO nanoparticles and improved the porosity and pore size of the membrane, as indicated by the findings of Zhi et al. (2015) [10]. Increasing the GO:CH ratio made the casting solution more viscous and increased its mass transfer resistance, resulting in reduction of porosity and pore radius. Similar conclusions were also found by Alkhozam et al. (2021) [11].

Table 3 also shows the membrane thickness, and as seen from the results, the thickness of the synthesized membranes varies between 52.01 μm and 63.42 μm . There is no clear trend in terms of thickness, and the thickness of all the membranes is very similar.

Table 3 Membrane thickness, pore size, porosity, and contact angle of the synthesized membranes

Membrane	Thickness (μm)	Porosity (%)	Membrane resistance	Pore radius (nm)	Contact angle ($^\circ$)
GC-0	53.87 \pm 2.3	57.35 \pm 2.6	17.85 \pm 2.0	11.41 \pm 1.4	87.4 \pm 3.6
GC-1	63.42 \pm 3.2	62.55 \pm 3.4	16.1 \pm 0.8	11.93 \pm 1.2	84.2 \pm 1.7
GC-2	53.80 \pm 2.7	62.25 \pm 3.7	11.60 \pm 0.6	12.28 \pm 1.4	81.0 \pm 2.6
GC-3	52.01 \pm 2.6	53.52 \pm 2.0	31.62 \pm 1.5	9.84 \pm 1.1	75.2 \pm 1.6
GC-4	55.00 \pm 2.8	62.09 \pm 3.8	84.22 \pm 4.4	12.12 \pm 0.7	83.2 \pm 2.4
GC-5	53.70 \pm 2.7	60.57 \pm 3.1	17.78 \pm 0.9	10.38 \pm 1.3	68.7 \pm 1.7
GC-6	52.61 \pm 2.6	65.10 \pm 3.8	7.61 \pm 0.4	14.15 \pm 1.7	82.2 \pm 1.6

3.3 Membrane morphology

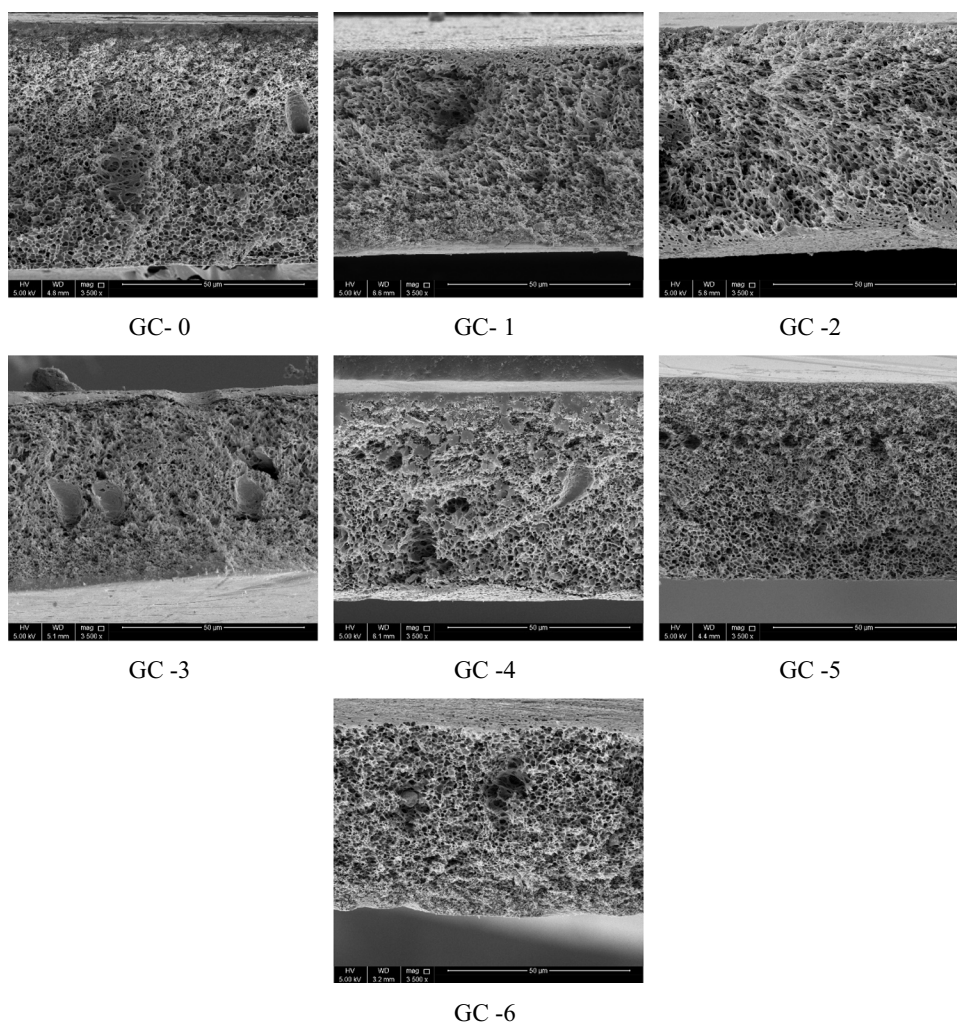
The morphology of the synthesized membranes was studied using the atomic force microscopy (AFM) and field emission scanning electron microscopy (FESEM) as per the methodology described in Sect. 2.6.1.

The cross-sectional SEM images of the pristine and GO-CH imbedded membranes are presented in Fig. 5. SEM image analysis of all synthesized membranes did not reveal any significant difference between the cross-section of the pristine membrane and the cross-section of the modified membranes as all membranes exhibited a sponge like structure. This usually occurs when the viscosity of the casting solution is high [12]. High viscosity of the casting solution will prevent solvent-non-solvent diffusion in the phase inversion or immersion-precipitation process which will suppress the formation of micro-void structure [13]. The SEM analysis also confirms uniform dispersion of the nanocomposite on the synthesized membranes as they did not show any agglomeration of the nanocomposite on the

membrane surfaces except for the GC-3 membrane where small agglomerations were observed. This might be attributed to higher concentration of GO-CH nanocomposite used for the fabrication of GC-3.

The surface morphology of the pristine and modified membranes was further studied using AFM analysis, and the results are shown in Fig. 6. The RMS roughness of the pristine membrane was found to be 9.58 nm. This value is very close to the surface roughness of pristine PSF membranes reported in various literatures [11, 14]. Figure 6 also shows the effect of increasing GO-CH nanocomposite concentration (GC-0, GC-1, GC-2, and GC-3) and the effect of increasing GO:CH ratio (GC-2, GC-4, GC-5, and GC-6) on the surface roughness. The result indicates that, while maintaining a GO:CH ratio of 1:0.5, increasing the concentration of GO-CH composite to 0.085 wt% (GC-2) in the membrane reduces the surface roughness to 5.15 nm. However, addition of 0.136 wt% (GC-3) nanocomposite increased the surface roughness to 26.94 nm. The initial reduction of surface roughness can be attributed to the low

Fig. 5 Cross-section SEM analysis of the synthesized membranes



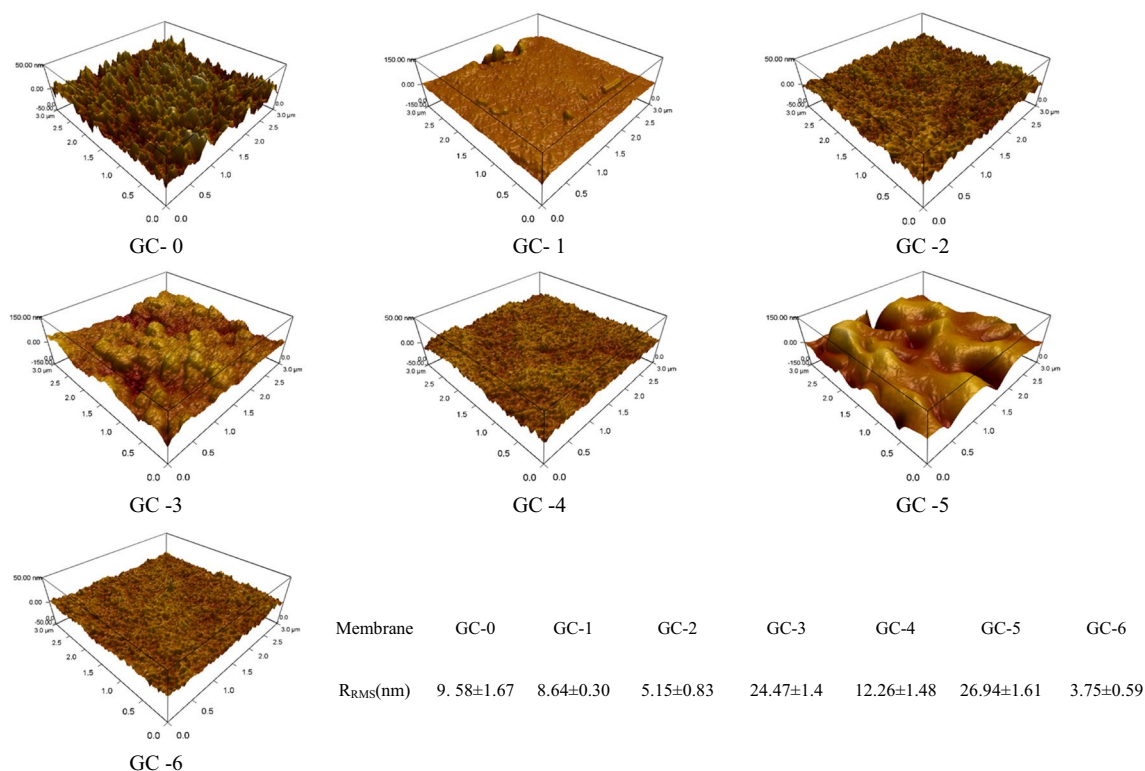


Fig. 6 AFM analysis of the pristine and modified membranes

electrostatic interaction and high compatibility between PSF and GO [15]. The deterioration of surface roughness after adding 0.136 wt% GO-CH nanocomposite (GC-3) can be attributed to slight agglomeration of the nanocomposites on the membrane surface, which was also observed in SEM analysis shown in Fig. 5. By reducing the GO:CH ratio to 1:0.1 and using 0.085 wt% GO-CH nanocomposite (GC-6), the surface roughness was reduced to 3.75 nm. However, at 0.085 wt% nanocomposite concentration, increasing the GO:CH ratio to 1:1 (GC-5) increased the surface roughness to 26.94 nm. This trend can be attributed to lack of compatibility between Psf and CH.

3.4 Pure water permeation flux

Water permeation flux studies were performed to investigate the effect of GO-CH nanocomposite concentration and GO:CH ratio in the nanocomposite. The effect of GO-CH concentration was studied by keeping the GO:CH ratio constant at 1:0.05 and altering the GO-CH concentration between 0, 0.034, 0.085, and 0.136 wt%. The results are summarized in Fig. 7(a). Figure 7(a) indicates that for a constant GO:CH ratio of 1:0.5, increasing the GO-CH concentration from 0 wt% (GC-0) to 0.085 wt% (GC-2) increases the permeate flux from 6.23 LMH/bar to 9.66 LMH/bar, corresponding to a 55% increase in water flux. However,

increasing the GO-CH concentration to 0.136 wt% (GC-3) decreased the permeate flux by 57%. This change in permeate flux can be related to the change in porosity, pore sizes, and contact angles shown in Table 3. Increasing the GO-CH concentration from 0 to 0.034 wt% improved the porosity, pore size, and hydrophilicity by 8.5%, 7.7%, and 7.3%, respectively. These improvements lowered the mass transfer resistance across the membrane for the water molecules, resulting in higher water flux for GC-2. Although increasing the GO-CH concentration to from 0.085 wt% to 0.136 wt% (GC-3) improved the hydrophilicity by 7.2%, deterioration of porosity and pore size by 14.0% and 19.8%, respectively, decreased the permeate flux. Thus, 0.085 wt% is deemed to be the best GO-CH concentration within the studied range.

The effect of GO:CH ratio on the permeate flux was studied by keeping the GO-CH concentration constant at 0.085 wt% and varying the GO:CH ratio between 1:0, 1:0.01, 1:0.05, and 1:1. The result of the study is shown in Fig. 7(b). As shown in Fig. 7(b), decreasing the GO-CH ratio from 1:0.05 (GC-2) to 1:0 (GC-4) decreases the permeate flux by 75.9%. However, increasing the GO:CH ratio from 1:0 (GC-4) to 1:0.01 (GC-6) improves the permeate flux by 535.7%. Further increment of GO:CH ratio from 1:0.01 (GC-6) to 1:1 (GC-5) deteriorates the permeate flux by 57.2%. These changes in the permeate flux can be explained by examining the porosity, pore radius, and contact angle

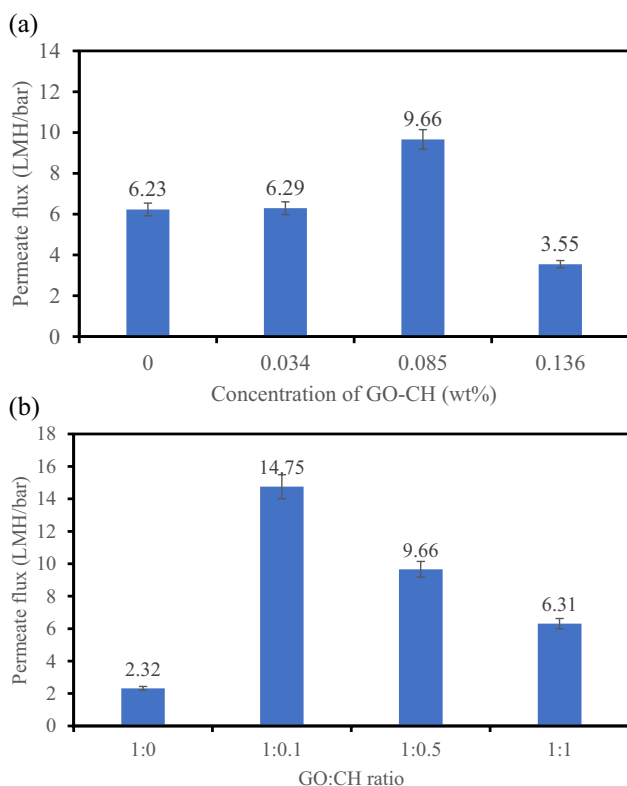


Fig. 7 Effect of (a) GO-CH nanocomposite concentration (at 1:0.5 GO:CH ratio) and (b) GO:CH ratio (at 0.085 nanocomposite concentration) on pure water permeate flux

data shown in Table 3. Using 0.085 wt% GO-CH nanocomposite with GO:CH ratio of 1:0 results in a porosity, pore radius, and contact angle of 60.09%, 12.12 nm, and 83.2°. Increasing the GO:CH ratio to 1:0.01 (GC-6) increases the porosity and pore radius to 65.10% and 14.15% and reduces the contact angle to 82.2°. These improvements reduce the mass transfer resistance and results in enhanced water permeation flux while using GC-6. Although increasing the GO:CH ratio to 1:1 reduces the contact angle to 68.7°, the deterioration of porosity and pore size to 60.57% and 10.38 nm, respectively, hence, increasing mass transfer resistance across the membrane and resulting in the reduction in permeate flux. Thus, during this study, the membrane modified with 0.085 wt% GO-CH, where the GO:CH ratio was 1:0.1, i.e., GC-6, showed the highest permeate flux.

3.5 Fouling study

The fouling study in terms of total fouling ratio (R_t), flux recovery ratio (FRR), reversible fouling ratio (R_r), and the irreversible fouling ratio (R_{ir}) was conducted according to the method discussed in Sect. 2.6. BSA was used as the model foulant, and the obtained results showed that the BSA rejection for the pristine membrane and the modified

Table 4 Fouling performance of the synthesized membranes

Membrane	FRR (%)	R_t (%)	F_{ir} (%)	F_r (%)
GC-0	61.89 ± 4.33	76.05 ± 4.56	38.11 ± 4.19	37.94 ± 4.17
GC-1	79.51 ± 5.57	24.61 ± 1.48	20.49 ± 2.25	4.13 ± 0.45
GC-2	81.61 ± 5.71	69.42 ± 5.16	18.39 ± 3.02	51.03 ± 5.61
GC-3	93.67 ± 6.55	53.64 ± 3.21	6.33 ± 0.70	47.32 ± 4.20
GC-4	80.31 ± 6.61	43.49 ± 2.60	19.69 ± 1.26	23.80 ± 2.61
GC-5	95.01 ± 6.65	65.40 ± 3.92	4.99 ± 0.54	60.41 ± 6.65
GC-6	80.73 ± 4.65	42.64 ± 3.56	19.27 ± 3.12	23.37 ± 2.57

membranes were < 99%. The results from the fouling study are presented in Table 4. The FRR, R_t , F_{ir} , and F_r of the pristine membrane (GC-0) were 61.89%, 76.05%, 38.11%, and 37.94%, respectively, while membrane modified using GO-CH nanocomposite resulted in improvement of all these parameters. GC-1 and GC-5 showed lowest R_t and F_{ir} of 24.61% and 4.99%, respectively, whereas the highest FRR and F_r of 95.01% and 60.41%, respectively, were obtained by GC-5. In general, out of the four tested parameters, GC-5 showed the best performance in terms of FRR, F_{ir} , and F_r . This can be attributed to the highest hydrophilicity of GC-5 as indicated by a contact angle of 68.7°, as shown in Table 3. This improved hydrophilicity will prevent BSA from forming stable bonds on the membrane surface and reduce irreversible fouling on the membrane surface which will improve FRR and F_r . Although GC-5 has the highest hydrophilicity, it also has the highest membrane roughness of 26.94 nm, as seen in Fig. 6. Rougher surfaces are expected to promote interaction with soluble foulants. However, for particulate foulants, the strength of interaction depends on the foulant size. In most cases, a higher particle size would fail to settle inside the crevices of a rough membrane and result in lower membrane fouling, as is the case in this study [16, 17]. Although the irreversible fouling was low for GC-5, the rougher surface of GC-5 made the membrane with the 2nd highest total fouling among all the tested membranes. Considering all the parameters, GC-5 is deemed to be the membrane with best anti-fouling performance.

3.6 Membrane performance for industrial wastewater treatment

The prepared membranes were tested for the COD rejection from an industrial wastewater. The COD rejection rate and corresponding permeate flux of the pristine and modified membranes are shown in Fig. 8. The pristine polysulfone membrane (GC-0) showed the lowest COD rejection efficiency of 29.32% with an average permeate flux of 3.74 LMH/bar. Incorporating 0.085 wt% GO increased COD rejection to 31.8%; however, it resulted in the lowest average permeate flux of 1.39 LMH/bar. Incorporating 0.085 wt%

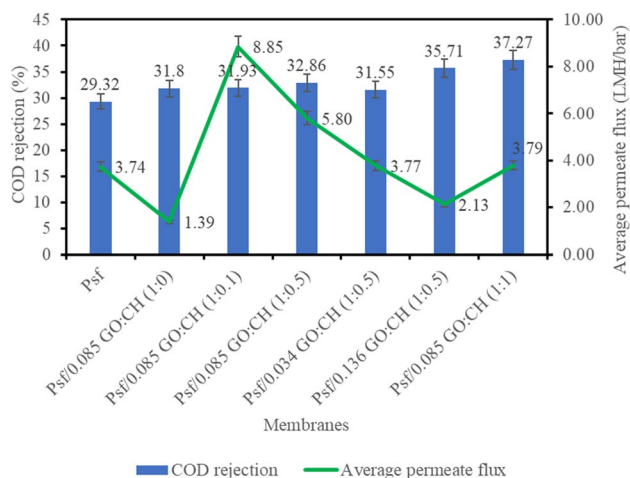


Fig. 8 COD removal efficiency of the synthesized membranes

GO-CH nanocomposite (GO:CH 1:0.1) improved the COD rejection slightly to 31.93% and resulted in the highest average permeate flux of 8.85 LMH/bar. At the same GO-CH concentration, increasing the GO:CH ratio to 1:1 improved the COD rejection to 37.27%; however, the average permeate flux decreased to 3.79 LMH/bar. While maintaining GO:CH ratio at 1:0.5, increasing GO-CH concentration to 0.136 wt% resulted in COD rejection to 35.71% with an average permeate flux of 2.13 LMH/bar. Thus, for COD rejection, increasing GO-CH concentration and GO:CH ratio improved COD rejection. These improvements in COD rejection can be attributed to improvement in hydrophilicity and reduction in pore sizes while using higher nanoparticle concentration and CH loading. For example, the membrane GC-5 showed the highest COD rejection rate, which was 27.1% higher than the pristine membrane owing to 6.4% reduction in pore size and 23.9% improvement in hydrophilicity, as shown in Table 3. The lower pore size prevented larger pollutants from crossing the transmembrane boundary, and higher hydrophilicity resulted in enhanced mass transfer resistance for the pollutants; thus, enhancing COD rejection. The membrane hydrophilicity and the pore size are also responsible for the variable average permeate flux. The effect of GO-CH

concentration and GO:CH ratio on pure water permeate flux has been discussed in Sect. 3.4.

3.7 Comparison with other membranes

Available data on the performance of different polysulfone ultrafiltration membranes doped with GO based nanocomposites published recently are summarized in Table 5. The table shows three key parameters: normalized rejection enhancement, normalized flux enhancement, and flux recovery rate while using the synthesized membranes. As seen from Table 5, the highest normalized rejection enhancement of 27.1% was achieved using the GC-5 membrane synthesized in this work. Moreover, the highest flux recovery rate of 95% was observed for the GC-6 membrane, which was also fabricated in this work. However, the greatest normalized flux enhancement of 300% was obtained by Vaghasia et al. (2022) who used GO-poly (MMA-co-GMA) to synthesize the polysulfone membrane. Among the membranes synthesized during this study, the GC-6 membrane showed 237% normalized flux enhancement. Although GC-5 showed 95% flux recovery rate and 27.1% COD rejection rate, the flux enhancement was only 1%. Since GC-5 shows considerable improvement in COD rejection (8.9%), membrane permeate flux (137%), and flux recovery rate (80%), thus, this is the membrane with optimum performance parameters.

4 Conclusion

In this study, GO-CH multifunctional nanocomposite was successfully synthesized and used to modify polysulfone membrane. The synthesized nanoparticles were rich in hydrophilic functional groups, including hydroxyl and carboxylic acid. Through FTIR and XRD analyses, the composition of synthesized GO-CH nanocomposite was confirmed. During the nanocomposite synthesis, the ratio of GO and CH was varied between 1:0, 1:0.1, 1:0.5, and 1:1. The concentration of GO-CH nanocomposite in the fabricated membrane was varied between 0 wt%, 0.034 wt%, 0.085 wt%, and 0.136 wt%. The surface morphology of

Table 5 Performance comparison between different polysulfone membranes modified with graphene oxide-based nanocomposites

Membrane nanofiller	Type of treated water	Rejection enhancement	Flux enhancement	Flux recovery rate	Reference
GO-poly (MMA-co-GMA)	1,000 ppm oil in water emulsion	0.3%	200%	88%	[18]
GO-DPPA	200 ppm BSA	6.4%	145%	80%	[19]
rGO-DDA	25 ppm HA	0%	-11%	89%	[20]
GO-SiO ₂	Rubber laden wastewater	15.1%	29%	58%	[21]
SPK-g-GO	Natural organic matter solution	10.4%	170%	90%	[22]
GO-CH (GC-6)	Industrial wastewater	8.9%	137%	80%	This work

the synthesized membranes was characterized with SEM and AFM. The FESEM showed no significant differences between the pristine and synthesized membranes. However, the AFM analysis showed reduction in surface roughness for the synthesized membranes. The synthesized membranes were tested for their permeability using a dead-end apparatus, and the highest flux of 14.75 LMH/bar was obtained by using the membrane doped with 0.085 wt% GO-CH at 1:0.1 GO:CH ratio (GC-6) due to higher membrane porosity, pore radius, and improved membrane hydrophilicity. Fouling study carried out with BSA indicated significant improvement in anti-fouling properties. Membrane prepared with 0.085 wt% GO-CH at 1:1 GO:CH ratio (GC-5) showed flux recovery rate of 95.01%, irreversible fouling of 4.99%, and reversible fouling of 60.41%. This improvement in anti-fouling performance can be attributed to improve membrane hydrophilicity and higher surface roughness where bigger BSA particles failed to enter the smaller crevice on membrane surface and form stronger bonds. The membrane performance was further tested for industrial wastewater treatment where GC-5 showed highest COD removal of 37.27% owing to its smaller pore radius and improved hydrophilicity. Therefore, by incorporating GO-CH multifunctional nanocomposite, the membrane hydrophilicity, fouling resistance, and COD removal efficiency were improved in the polysulfone membrane.

Acknowledgements The authors would like to thank Central Laboratories Unit (CLU) located at Qatar University for their assistance during characterization of the membrane.

Author contribution Ahmed Toky Yasir: methodology, investigation, writing—original draft, and validation. Abdelbaki Benamor: writing—review and editing, formal analysis, and project administration. Alaa H. Hawari: writing—review and editing, formal analysis, and project administration. Ebrahim Mahmoudi: conceptualization and visualization.

Funding Open Access funding provided by the Qatar National Library. This research is made possible by graduate sponsorship research award (GSRA7-1-0510-20046) from Qatar National Research Fund (QNRF). The publication of this article was funded by Qatar National Library (QNL). The statements made herein are solely the responsibility of the authors.

Data availability The data that support the findings of this study are not openly available due to reasons of sensitivity and are available from the corresponding author upon reasonable request.

Declarations

Competing interests The authors declare no competing interests.

Open Access This article is licensed under a Creative Commons Attribution 4.0 International License, which permits use, sharing, adaptation, distribution and reproduction in any medium or format, as long as you give appropriate credit to the original author(s) and the source, provide a link to the Creative Commons licence, and indicate if changes were made. The images or other third party material in this article are

included in the article's Creative Commons licence, unless indicated otherwise in a credit line to the material. If material is not included in the article's Creative Commons licence and your intended use is not permitted by statutory regulation or exceeds the permitted use, you will need to obtain permission directly from the copyright holder. To view a copy of this licence, visit <http://creativecommons.org/licenses/by/4.0/>.

References

1. E. Mahmoudi, L.Y. Ng, M.M. Ba-Abbad, A.W. Mohammad, Novel nanohybrid polysulfone membrane embedded with silver nanoparticles on graphene oxide nanoplates. *Chem. Eng. J.* **277**, 1–10 (2015). <https://doi.org/10.1016/j.cej.2015.04.107>
2. L. Shao, X. Chang, Y. Zhang, Y. Huang, Y. Yao, Z. Guo, Graphene oxide cross-linked chitosan nanocomposite membrane. *Appl. Surf. Sci.* **280**, 989–992 (2013). <https://doi.org/10.1016/j.apsusc.2013.04.112>
3. H. Zhang et al., Synthesis and characterization of TiO₂/graphene oxide nanocomposites for photoreduction of heavy metal ions in reverse osmosis concentrate. *RSC Advances* **8**(60), 34241–34251 (2018). <https://doi.org/10.1039/C8RA06681G>
4. I. Sengupta, S. Chakraborty, M. Talukdar, S. Pal, and S. Chakraborty, Thermal reduction of graphene oxide: how temperature influences purity. *J. Mater. Res.* 1–10 (2018) <https://doi.org/10.1557/jmr.2018.338>
5. X. Wang, R. Tang, Y. Zhang, Z. Yu, and C. Qi 2016 Preparation of a novel chitosan based biopolymer dye and application in wood dyeing (in eng). *Polymers (Basel)*. **8** (9) (2016) <https://doi.org/10.3390/polym8090338>
6. X. Song, S. Cui, Z. Li, Y. Jiao, C. Zhou, Fabrication of chitin/graphene oxide composite sponges with higher bilirubin adsorption capacity. *J. Mater. Sci. Mater. Med.* **29**(7), 108 (2018). <https://doi.org/10.1007/s10856-018-6107-8>
7. S. Ghazizadeh, P. Duffour, N. Skipper, M. Billing, Y. Bai, An investigation into the colloidal stability of graphene oxide nanolayers in alite paste. *Cement Concrete Res.* **99**, 116–128 (2017). <https://doi.org/10.1016/j.cemconres.2017.05.011>
8. A.G.B. Pereira, F.H.A. Rodrigues, A.T. Paulino, A.F. Martins, A.R. Fajardo, Recent advances on composite hydrogels designed for the remediation of dye-contaminated water and wastewater: a review. *J. Clean. Prod.* **284**, 124703 (2021). <https://doi.org/10.1016/j.jclepro.2020.124703>
9. J. Yang, X. Chen, J. Zhang, Y. Wang, H. Wen, J. Xie, Role of chitosan-based hydrogels in pollutants adsorption and freshwater harvesting: a critical review. *Int. J. Biol. Macromol.* **189**, 53–64 (2021). <https://doi.org/10.1016/j.ijbiomac.2021.08.047>
10. S.-H. Zhi, R. Deng, J. Xu, L.-S. Wan, Z.-K. Xu, Composite membranes from polyacrylonitrile with poly(N, N-dimethylaminoethyl methacrylate)-grafted silica nanoparticles as additives. *React. Funct. Polym.* **86**, 184–190 (2015). <https://doi.org/10.1016/j.reactfunctpolym.2014.09.004>
11. A. Alkhouzaam, H. Qiblawey, Novel polysulfone ultrafiltration membranes incorporating polydopamine functionalized graphene oxide with enhanced flux and fouling resistance. *J. Membrane Sci.* **620**, 118900 (2021). <https://doi.org/10.1016/j.memsci.2020.118900>
12. Z. Wang, J. Ma, Q. Liu, Pure sponge-like membranes bearing both high water permeability and high retention capacity. *Desalination* **278**(1), 141–149 (2011). <https://doi.org/10.1016/j.desal.2011.05.023>
13. C.A. Smolders, A.J. Reuvers, R.M. Boom, I.M. Wienk, Microstructures in phase-inversion membranes Part I Formation of macrovoids. *J. Membrane Sci.* **73**(2), 259–275 (1992). [https://doi.org/10.1016/0376-7388\(92\)80134-6](https://doi.org/10.1016/0376-7388(92)80134-6)

14. M.R. Jamalludin et al., Antifouling polysulfone membranes blended with green SiO₂ from rice husk ash (RHA) for humic acid separation. *Chem. Eng. Res. Design* **114**, 268–279 (2016). <https://doi.org/10.1016/j.cherd.2016.08.023>
15. R. Rezaee et al., Fabrication and characterization of a polysulfone-graphene oxide nanocomposite membrane for arsenate rejection from water. *J. Environ. Health. Sci. Eng.* **13**(1), 61 (2015). <https://doi.org/10.1186/s40201-015-0217-8>
16. M. Zhang et al., Effects of hydrophilicity/hydrophobicity of membrane on membrane fouling in a submerged membrane bioreactor. *Bioresour. Technol.* **175**, 59–67 (2015). <https://doi.org/10.1016/j.biortech.2014.10.058>
17. L. Chen, Y. Tian, C.-Q. Cao, J. Zhang, Z.-N. Li, Interaction energy evaluation of soluble microbial products (SMP) on different membrane surfaces: role of the reconstructed membrane topology. *Water Research.* **46**(8), 2693–2704 (2012). <https://doi.org/10.1016/j.watres.2012.02.030>
18. R. Vaghasia, B. Saini, A. Dey, "Synergetic effect of graphene oxide and poly(MMA-co-GMA) copolymer on PSF ultrafiltration membrane for the remediation of potential environmental contaminants. *J. Mole. Liquids* **359**, 119346 (2022). <https://doi.org/10.1016/j.molliq.2022.119346>
19. Z. Xu et al., Azido-group functionalized graphene oxide/polysulfone mixed matrix ultrafiltration membrane with enhanced interfacial compatibility for efficient water and wastewater treatment. *Sep. Purif. Technol.* **283**, 120162 (2022). <https://doi.org/10.1016/j.seppur.2021.120162>
20. A. Alkhouzaam, H. Qiblawey, Synergetic effects of dodecylamine-functionalized graphene oxide nanoparticles on antifouling and antibacterial properties of polysulfone ultrafiltration membranes. *J. Water Process Eng.* **42**, 102120 (2021). <https://doi.org/10.1016/j.jwpe.2021.102120>
21. T.D. Kusworo et al., Photocatalytic antifouling nanohybrid polysulfone membrane using the synergetic effect of graphene oxide and SiO₂ for effective treatment of natural rubber-laden wastewater. *J. Membrane Sci.* **657**, 120663 (2022). <https://doi.org/10.1016/j.memsci.2022.120663>
22. M. Kumar, H.M. Baniowda, N. Sreedhar, E. Curcio, H.A. Ararat, Fouling resistant, high flux, charge tunable hybrid ultrafiltration membranes using polymer chains grafted graphene oxide for NOM removal. *Chem. Eng. J.* **408**, 127300 (2021). <https://doi.org/10.1016/j.cej.2020.127300>